Electron states of uniaxially strained graphene

Hiroki Shioya[1†], Saverio Russo[2], Michihisa Yamamoto[1], Monica F. Craciun[2] and Seigo Tarucha[1,3].*

1. Department of Applied Physics, University of Tokyo, Tokyo, Japan

2. Center for Graphene Science, College of Engineering, Mathematics and Physical Sciences, University of Exeter, Exeter EX4 4QF, UK

3. Center for Emergent Matter Science (CEMS), RIKEN, Wako, Saitama, Japan

We report an experimental study of electron states and the resulting electronic transport properties of uniaxially strained graphene. For this study we developed a novel strain application method that is compatible with the planar device technology. We identify the value of the strain induced in graphene by Raman spectroscopy and show with atomic force microscopy that its topography consists of wrinkles up to 4nm height aligned along the direction of the applied strain. Transport experiments reveal a broadening of the charge neutrality region and the convergence of Landau-levels to multiple Dirac points in Landau-fan diagrams. These observations are consistent with large fluctuations of the scalar potential via the strain-induced wrinkles, which is experimentally observed for the first time.

KEYWORDS

Graphene, uniaxial strain, straintronics, planar device structures, strain induced potentials, Landau-fan diagram.

Graphene[1,2] consists of a single layer of carbon atoms with honeycomb lattice structure. This system is a unique mechanically flexible two dimensional conductor, and its unusual electronic properties can be modified with mechanical deformations. For example, by simply controlling the strain it is possible to modulate its opto-electronic properties[3-5], and it has also been theoretically predicted that a bandgap can be opened in the otherwise gapless energy dispersion of graphene[6-8].

To date, most of the experimental methods used to engineer strain in graphene exploit a curvature-induced strain controlled by the bending radius of a flexible substrate on to which the graphene is attached. However, with this method it is only possible to induce modest levels of strain which are far from the values needed, for example, to open an energy gap[6-8]. For this reason, the field of graphene straintronics – that is strain controlled optical and electrical response – has yet to deliver much impact in fundamental science. Strain engineered in planar graphene on rigid substrates was recently demonstrated using the shrinkage of thin films of evaporated metal (Ni) pad and organic insulating materials deposited on to graphene[9]. This offers a way to achieve the needed strain values to observe significant modifications of the opto-electronic properties, with potentially more than 20% strain applied[10] without slippage of graphene. However, the recrystallization of Ni-pads by electron beam irradiation is not ideally suited for studying the electrical transport properties in strained graphene since the electrical

contact between graphene and the metal degrades irreversibly upon the electron irradiation. Hence a new method for inducing strain in graphene is needed to assess the modification of the electrical properties in the material.

In this letter we present an experimental study of the modification of the electrical transport properties in graphene upon applying uniaxial strain in a planar configuration with a new strain application method. With Raman spectroscopy we characterize the value of the strain induced by the Ni-contacts, and with atomic force microscopy we show that strain changes the topography of graphene dramatically with the formation of wrinkles up to 4 nm in height aligned the direction of strain. In the magneto-conductance we observe a broadening of the current *vs*. back gate voltage characteristics caused by the strain-induced redistribution of charge carriers by local energy level shifts in the conduction channel. Contrary to the case of charge impurity-broadened Dirac peak, we show that even in the presence of uniaxial strain the charge carrier mobility remains large enough to observe multiple onsets of Shubnikov-de Haas oscillations originating from different gate voltages in the Landau fan diagram. This result is also in contrast with the simply broadened charge neutrality point associated with the electron and hole puddles induced by natural corrugations[11]. Our observations suggest that the wrinkles of uniaxially strained graphene induce domains of strain, accompanying a domain structure of the scalar potential that shifts the charge neutrality point, which is experimentally observed for the first time. Since uniaxial strain can be considered as a building block of more complex strain patterns, our studies are a first step towards graphene-based straintronics, showing experimentally that strain can also modulate a scalar potential.

Strained graphene samples were fabricated using mechanically exfoliated graphene onto a 285 nm thick layer of SiO_2 grown on heavily p-doped Si substrates, which serve as a back gate electrode. Single layer graphene flakes are selected by analyzing the intensity of the green light of optical micrograph pictures[12] and the 2D-band of the Raman spectra. To engineer strain in graphene we deposit pads of highly stressed Nickel (Ni). These are defined at the two ends of graphene flakes (separated by 2 to 2.5 μm) by standard electron-beam lithography, electron beam evaporation and lift-off processes.

Evaporated metal films are known to possess high levels of stress. Furthermore, the higher the melting temperature of a material possesses the higher the stress that can be attained upon deposition[13-15], and based on previous studies[13-15], we have identified Ni as a suitable material to induce strain in graphene. The thickness of the metal film is another parameter that offers direct control over the stress of the deposited metal, with thicker Ni film undergoing higher levels of tensile stress, making it possible to stretch graphene between two contacts (see supplementary information). Ultimately, when the stress of the metal film exceeds the graphene/Ni adhesion, we find that the evaporated film detaches from the graphene releasing all the strain induced by the Ni pads. Axial loading of graphene is attained in the direction connecting the centers of the two Ni pads resulting in uniaxial strain (see Figure 1a). Furthermore, we use Ni as an electronic contact to ascertain the evolution of the electrical properties of graphene undergoing uniaxial strain. We have studied more than 10 samples and in this letter we focus on four representative devices, which capture the overall trend of uniaxially strained graphene.

To determine the applied strain in graphene we employed Raman spectroscopy. Figure 1b shows representative Raman G-peaks measured in four distinct strained graphene devices.

Contrary to the case of unstrained graphene where the G-peak is a single peak centered at around 1580 cm^{-1} [16], in all the studied samples we observe that the G-peak shape is the superposition of two distinct red shifted peaks. This observation is consistent with strain induced lifting of the degeneracy of the peaks originally forming the G-peak. Furthermore, the fact that these peaks are red shifted compared to the unstrained case indicates that graphene is being stretched by the Ni pads. To estimate the degree of the applied strain we follow the model developed in Ref [17]. We find that the ratio of the stretching along the channel (ε_{ll}) to the compression perpendicular to that (ε_{tt}), is $|\varepsilon_{tt}/\varepsilon_{ll}| = 0.224 \pm 0.041$ (mean value of four samples ± standard deviation of them). This value is comparable to the Poisson's ratio of graphene, 0.186[18], confirming that the type of strain applied in these devices is uniaxial and tensile.

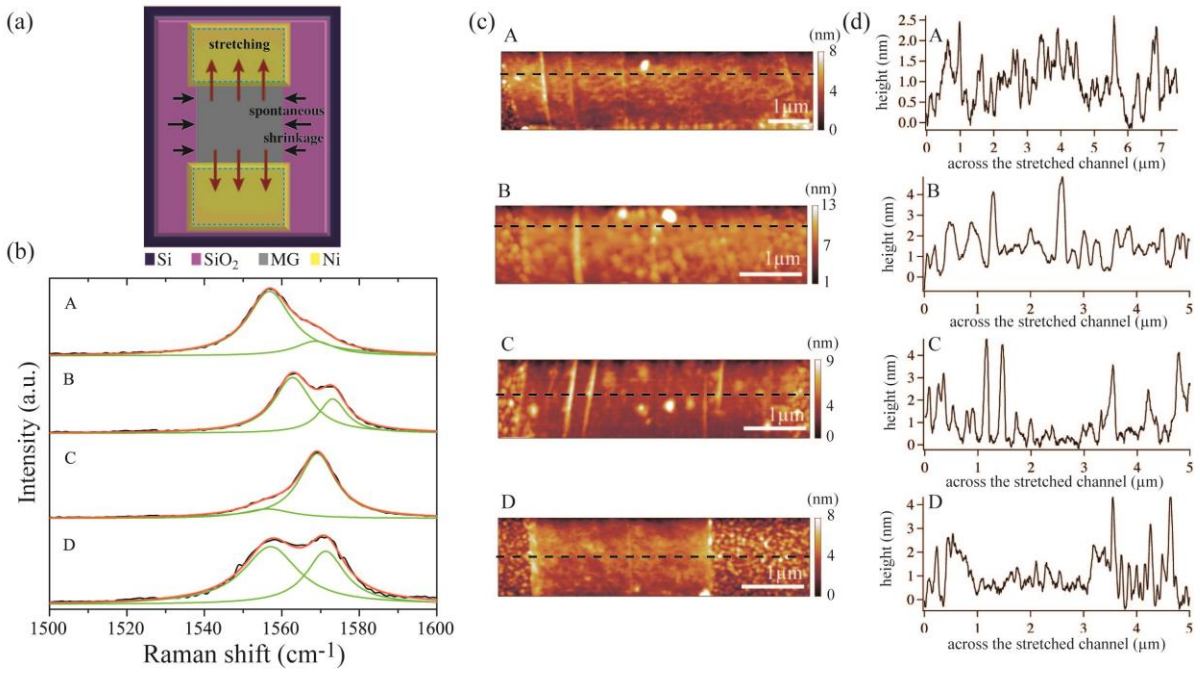

Figure 1. (a) Schematic diagram of the studied uniaxially strained graphene sample. We employ evaporated Ni film that is known to possess high levels of tensile stress. The graphene channel between two Ni pads is stretched uniaxially along the line connecting the pads and shrinks

spontaneously by the Poisson effect. (b) G-peak Raman spectra of the uniaxially strained graphene. All spectra show red shift and can be fitted by two Lorenz peaks. We employ variables of ε_{ll} and ε_{tt} (the unit:%) to express strain for longitudinal and transverse directions to the direction along the strained channel, respectively. Their positive/negative values mean tensile/compressive strain. The evaluated strains are A (Ni film 170nm):(ε_{ll}, ε_{tt})=(0.65, -0.11) and $|\varepsilon_{tt}/\varepsilon_{ll}|$=0.173, B(Ni film 175nm):(ε_{ll}, ε_{tt})=(0.51, -0.13) and $|\varepsilon_{tt}/\varepsilon_{ll}|$=0.252, C(Ni film 222nm):(ε_{ll}, ε_{tt})=(0.69, -0.14) and $|\varepsilon_{tt}/\varepsilon_{ll}|$=0.198, D(Ni film 207nm):(ε_{ll}, ε_{tt})=(0.70, -0.19) and $|\varepsilon_{tt}/\varepsilon_{ll}|$=0.275. (c) AFM images of the uniaxially strained graphene channels in samples A, B, C, and D. Strain induced wrinkles along the stretching direction are confirmed in all samples. (d) The cross sections of the height profiles corresponding to the broken lines indicated in (c). Small corrugations less than 1nm height as well as large wrinkles up to a few nm height are observed.

The surface morphology of the uniaxially strained graphene is investigated by an atomic force microscope (AFM) and the representative results are shown in Figure 1c. We observe strain induced large and small wrinkles[19, 20] preferentially aligned in the direction of the applied strain, typically of the order of nanometer in height. Wrinkles emerge only when the applied tensile strain exceeds the critical value of strain needed to generate them[20]. These wrinkles are consistent with the spontaneous shrinkage perpendicular to the stretching direction, and they are reminiscent of the wrinkles seen when a tissue is pulled by two sides.

In the following we focus on the electrical properties of strained graphene where the flow of current is in the direction of strain. Figure 2 shows representative source-drain current (I_{ds}) *vs.* back gate voltage (V_{bg}) curves for two representative strained samples (A and D), measured at

around 1.5K and using a constant V_{ds} value of 100μV, that is smaller than the thermal energy k_BT to avoid undesired signals caused by non-equilibrium phenomena (I_{ds}-V_{bg} characteristics for more samples are shown in the supplementary information). In all the uniaxially strained cases we observe a broadening of the charge neutrality point from a well-defined value of V_{bg} in unstrained graphene (see Figure 2a) to a large range of V_{bg} which increases with the strain induced in graphene, reaching ΔV_{bg} = 50V for the sample with the largest strain, where ΔV_{bg} is the difference between the highest and the lowest charge neutral point indicated by two arrows on the V_{bg} axis (see Figure 2b, c). Ti/Au electrodes are employed in the case of unstrained graphene, and the corresponding Raman spectrum of the G-peak confirms the absence of externally applied strain (see supplementary information).

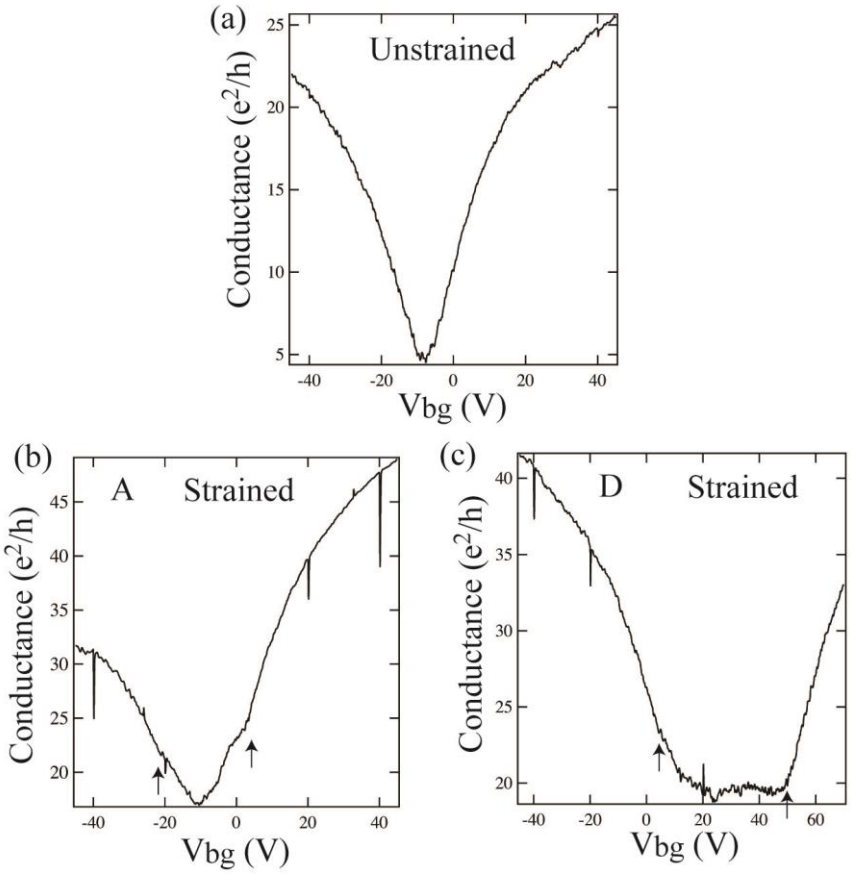

Figure 2. Panels (a-c) show the I_{ds}-V_{bg} characteristics of pristine graphene in the absence of externally applied strain (a) and with different magnitudes of applied uniaxial strain (b,c). Black arrows indicate the highest and lowest Dirac points in the V_{bg} axis judged by these measurements.

The electron(hole) mobility in the strained samples are comparable to the values typically measured in unstrained mechanically exfoliated graphene on SiO_2, and the values of samples A, B, C and D are 12200(7200), 7900(4600), 8100(5000) and 3000(2700) (cm^2/Vs), respectively. We further proceed to study the magneto-conductance of strained graphene at T=1.5K in the presence of a magnetic field of 10T perpendicular to the plane of the sample, see Figure 3. Clear steps of the magneto-conductance corresponding to the integer quantum Hall sequence of graphene are measured in sample A. The observed typical charge carrier mobility values upon strain together with a clear integer quantum Hall sequence developing upon applying a perpendicular magnetic field indicate that the broadening of the V-shaped I_{ds}-V_{bg} curves is not due to disorder induced states[21, 22].

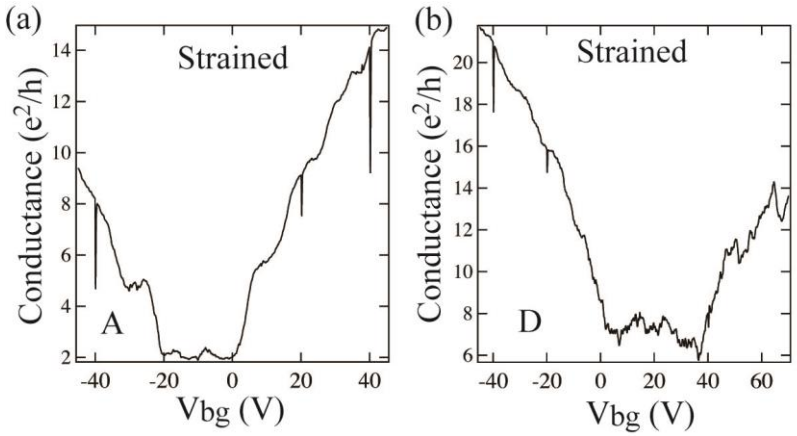

Figure 3. (a,b) show the I_{ds}-V_{bg} characteristics of uniaxially strained graphene under the magnetic field of 10T for sample A, and D, respectively.

Figure 4 shows color plots of the derivative of the source-drain current with respect to the back gate voltage as a function of V_{bg} and for applied magnetic field ranging from 0T to 10T. We found that lines fan out from plural points of V_{bg} at B=0T. To understand the physical origin of these lines, we conduct a fit to the theoretically expected slope of Landau levels for various filling factors and neutrality point corresponding to the convergence at B=0T for each group of lines. The good agreement between the theoretically expected slopes and the experimental data shows that the dispersing lines of Figure 4a truly are Landau levels of Dirac fermions. In the case of larger strain, such as sample D, the broad neutrality region seen in the I_{ds} *vs.* V_{bg} (e.g. $\Delta V_{bg}^{D} \approx 2\Delta V_{bg}^{A}$, see Figure 2(b,c)) is associated with a large number of convergence point in a Landau fan diagram (see Figure 4b). Indeed, the region in V_{bg} over which the Landau levels fan out at B=0T is consistent with the ΔV_{bg} neutrality region observed in the I_{ds}-V_{bg} curves in Figure 2, and indicates that the density distribution has plural local minima. In addition, the larger number of lines is found in sample D, compared with those of sample A. This is probably due to the larger number of Dirac points in the conduction channel of sample D. Flows of lines converging to plural charge neutral points at B=0T support the existence of plural charge neutrality points (see Figure 4). We also found that the larger is the ratio of $|\varepsilon_{tt}/\varepsilon_{ll}|$ the wider is the range of convergence points in the Landau fan diagram. This indicates that highly compressed structures or corrugated wrinkles are related to the plural convergence points in the Landau fan diagram or charge distributions in the strained graphene channels.

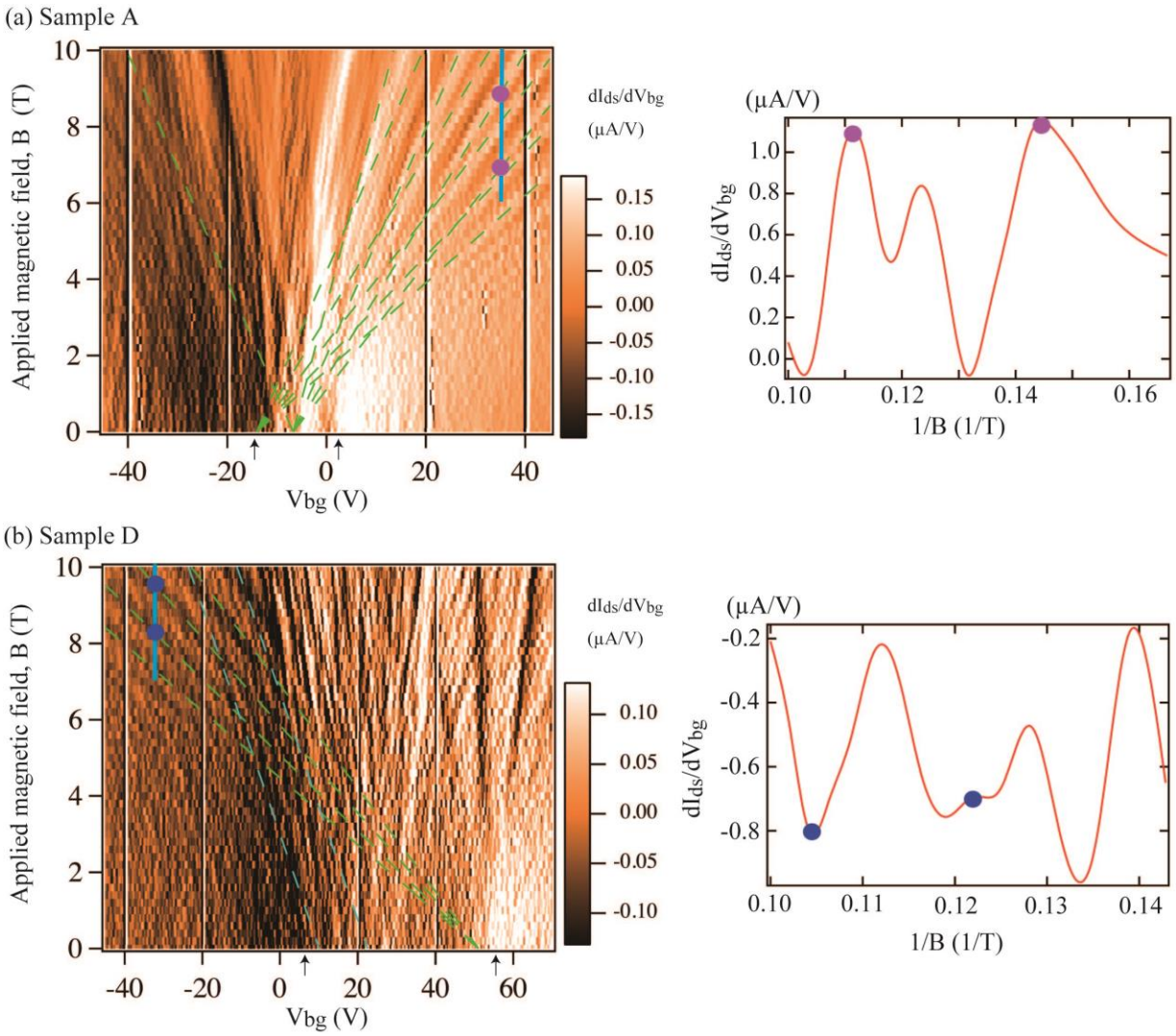

Figure 4. (a, b) show Landau-fan diagrams and SdH oscillations along the blue lines in the diagram of uniaxially strained graphene samples for sample A, and D, respectively. The ΔV_{bg} highlighted by black arrows is the back gate region over which plural convergence points in the Landau-fan diagrams are observed. Green dashed lines indicate the Landau level sequences. Blue dashed lines in (b) have slope of a Landau level followed by flows of finer lines converging to the same points of around 10V and 20V at B=0T, which are charge neutrality points. The charge densities in the strained channels calculated by the magnetic frequency evaluated from SdH oscillations, which are 3.05×10^{12} (1/cm^2) and 5.48×10^{12} (1/cm^2) for sample A and sample D,

respectively. These values show good agreement with the evaluation using a planar capacitance model, which are 3.78×10^{12} (1/cm^2) and 6.20×10^{12} (1/cm^2) for sample A and sample D, respectively.

There are multiple factors that are known to contribute to the creation of electron-hole puddles in graphene samples. Unwanted contamination during the fabrication process is a common cause of electron-hole puddles. Since the fabrication conditions are identical for strained and unstrained samples, this is the unlikely reason for the observed broadening of the V-shaped I_{ds}-V_{bg}. Low-energy disorder states, known to lead to localization of charge carriers, could potentially be another cause of broadening of the V-shaped I_{ds}-V_{bg}. However, in this case a negative magneto-resistance has to be expected[23] and this is in contrast with our experimental findings. Therefore, disorder-induced localized states also cannot explain the observed broadening of the V-shaped I_{ds}-V_{bg}. A third mechanism that induces electron-hole puddles is related to the change in the topography of the samples. More specifically, the emergence of wrinkles in graphene will cause spatial variation of the capacitive coupling to the back gate. However, this effect cannot account for the observed broadening of the neutrality region ΔV_{bg}. This is because the modulation in total charge density due to the experimentally measured wrinkles is less than 1% since the wrinkles have a height of just a few nanometers whereas the SiO_2 is 285 nm thick. A fourth mechanism potentially relevant for the generation of electron-hole puddles could be flexoelectricity. However, recent theoretical advances have shown that only systems with lower symmetry have a higher dipole moment and a considerable flexoelectricity has to be expected[24]. The AFM characterization of our devices shows a very limited level of

random bumps with the diameter of a hundred nano-meters in the topography of graphene, which is a much larger diameter than the nano-hones in which flexoelectricity is relevant effect[24]. In contrast to nano-hones, the strained graphene channels presented in this manuscript have an inversion symmetric structure. Hence flexoelectricity is expected to play a negligible role[24].

Having excluded a potential role of some mechanisms for the formation of electron-hole puddles (i.e. contamination, disorder and spatially varied capacitance, flexoelectricity), we note that in strained graphene, an alternative physical mechanism can lead to the broadening of the neutrality region. It is well-known that mechanical deformations of the graphene lattice generate vector and scalar potentials that act on the charge carriers[25, 26]. Wrinkles found in the AFM measurements clearly show that their size varies and we observe that the sample with the highest value of $|\varepsilon_{tt}/\varepsilon_{ll}|$ has the largest density of wrinkles. This highly packed wrinkle structure would be a reason to cause high levels of bending of carbon lattices in the strained graphene. We note that the magnitude of tensile strain can be inhomogeneous due to the curvature or, more precisely, to the wavelength of the wrinkles as shown in the paper of Ref [20], in which an expression for the magnitude of the tensile strain as a function of the wavelength of the wrinkles is derived. Hence, the tensile strain in the samples is not uniform. The position dependent strain could be due to the specific boundary conditions[20]. At the two ends, the graphene is covered by a metal film, which will affect the shrinking as a Poisson's effect resulting in a position dependent strain of graphene. Deformations associated with wrinkles of graphene generate position dependent potentials, which have been theoretically shown to enhance the electron-hole puddles near the neutrality point[11]. This charge inhomogeneity can broaden the peak shape of I_{ds}-V_{bg} curves. Strain can therefore smear the density of states near Dirac point. We also note that small curvature would not much affect the interatomic hopping elements because the sample with natural corrugation

does show plural convergence points in the Landau fan diagram as shown in many previous studies.

In all the studied uniaxially strained graphene samples we have observed the presence of wrinkles aligned in the direction of the applied strain (see Figure 1). The dramatic change in the topography of the graphene flakes upon strain is due to lattice deformation which are bound to induce locally different Dirac points in the energy level or charge inhomogeneity.

The discrepancies between clear quantum Hall steps and unclear ones shown in Figure 3 can be explained by the presence of a broad spatial distribution of Dirac points caused by the spatial distribution of the scalar potential induced by the strain. In the case of the widely broadened distribution of Dirac points, the conduction channels originated from different charge densities, which correspond to the domain of strain, are mixed and then the total conductance measured in the transport experiments are superposed values because the charge density in each domain is uniform as shown by the formation of Landau levels in Figure 4. Therefore, multiple convergence points in the Landau fan diagram are associated with more complex magneto-conductance characteristics and higher conductance values.

The experimental evidence that uniaxial strain induces the formation of wrinkles in planar graphene transistors with Ni contacts is also of fundamental importance for the research area focused on spin-electronics. Since early experiments of spin injection and detection in mechanically exfoliated graphene spin-valve devices, it was found that the spin relaxation length in graphene was much shorter than the theoretically expected value[27, 28]. Our experiments indicate that stress in the high melting point magnetic contacts may be inducing a roughening of

the topography of graphene. This would result in widely spatial dependent scalar and vector potentials which would ultimately reduce the spin relaxation length.

In conclusion, we demonstrated a new strain application method and by employing it we measured electrical transport properties of uniaxially strained graphene. The broadened peak shape near the Dirac point in the I_{ds}-V_{bg} curve and plural convergence points in the Landau-fan diagram are observed. These findings can be attributed to a wide spatial variation of the Dirac point in strained graphene due to the position dependent scalar potential, which is experimentally confirmed for the first time. Our experiments are the first magneto-transport experiments in uniaxially strained graphene on a planar substrate, and constitute a first step towards graphene-based strain engineering.

Methods

Sample preparation

In sample preparation samples are fabricated using mechanically exfoliated graphene onto a 285 nm thick layer of SiO_2 grown on heavily p-doped Si substrates, which serve as a back gate electrode. Single layer graphene flakes are selected by analyzing the intensity of the green light of optical micrograph pictures[12] and the 2D-band of the Raman spectra. To engineer strain in graphene we deposit pads of highly stressed Nickel (Ni). These are defined at the two ends of graphene flakes (separated by 2 to 2.5 μm) by electron-beam lithography (Elionix 7700 system) using the electron beam resist NANO 950 PMMA A6 (MicroChem Corp.) spin-coated at 4000 rpm for 50 seconds on the samples, followed by electron beam evaporation and lift-off processes.

Measurements of Raman spectrum

We used a commercially available system NRS-1000 (JASCO corp.) with the excitation wavelength of 532 nm and laser spot size around 2μm and incident power of less than 1mW to avoid damaging the graphene. The grating is 1800 grooves/mm and the spectral resolution is approximately 1 cm^{-1}.

Supporting Information.

This material has supplementary material file, which is available free of charge via the Internet at http://pubs.acs.org.

AUTHOR INFORMATION

Corresponding Author

Hiroki Shioya

shioya@meso.t.u-tokyo.ac.jp

University of Tokyo

Present Addresses

†Institute of Scientific and Industry Research, Osaka University, Osaka, Japan

shioya@sanken.osaka-u.ac.jp

ACKNOWLEDGMENT

The authors would like to acknowledge useful discussion with Prof. T.Osada on our experimental results.

H.S. acknowledges financial support from GCOE for Phys. Sci. Frontier and from Project for Developing Innovation Systems, MEXT, Japan.

S.R. and M.F.C acknowledge financial support from EPSRC (Grant no. EP/J000396/1, EP/K017160/1, EP/K010050/1, EPG036101/1, EP/M001024/1, EPM002438/1) and from Royal Society international Exchanges Scheme 2012/R3 and 2013/R2.

M.Y. acknowledges financial support from MEXT KAKENHI "Science of Atomic Layers".

S.T. acknowledges financial support from JST Strategic International Cooperative Programs (DFG-JST and EPSRC-JST) and Grants-in-Aid for Scientific Research S (No. 26220710).

REFERENCES

1. Novoselov, K.S., Geim, A.K., Morozov, S.V., Jiang, D., Katsnelson, M.I., Grigorieva, I.V., Dubonos, S.V. and Firsov, A.A., Two-dimensional gas of massless Dirac fermions in grapheme, Nature **2005**, 438, 197-200

2. Zhang, Y., Tan, Y.-W., Stormer, H.L. and Kim, P., Experimental observation of the quantum Hall effect and Berry's phase in grapheme, Nature **2005,** 438, 201-204

3. Pereira, Vitor M., and Castro Neto, A.H., Strain Engineering of Graphene's Electronic Structure, Phys. Rev. Lett. 2009, 103, 046801-046804

4. Vozmediano, M.A.H., Katsnelson, M.I., and Guinea, F., Gauge fields in graphene, Phys. Rep. **2010**, 496, 109-148

5. Guinea, F., Strain engineering in graphene, Solid State Communications, **2012**, 152, 1437-1441

6. Montambaux, G., Piechon, F., Fuchs, J.-N., and Goerbig, M.O., Merging of Dirac points in a two-dimensional crystal, Phys. Rev. B **2009**, 80, 153412-153415

7. Pereira, V.M., and Castro Neto, A.H., Tight-binding approach to uniaxial strain in graphene, Phys. Rev. B **2009**, 80, 045401-045408

8. Guinea, F., Katsnelson, M.I., and Geim, A.K., Energy gaps and a zero-field quantum Hall effect in graphene by strain engineering, Nat. Phys. **2009**, 6, 30-33

9. Shioya, H., Craciun, M. F., Russo, S., Yamamoto M., and Tarucha, S., Straining graphene using thin film shrinkage methods, NanoLett. **2014**, 14, 1158-1163

10. Lee, C., Wei, X., Kysar, J.W., and Hone, J., Measurement of elastic properties and intrinsic strength of monolayer graphene, Science 2008, 321, 385-388

11. Gibertini, M., Tomadin, A., Guinea, F., Katsnelson, M. I., and Polini, M., Electron-hole puddles in the absence of charged impurities, Phys. Rev. B **2012** (R) 85, 201405-201409

12. Blake, P., Hill, E.W., Castro Neto, A.H., Novoselov, K.S., Jiang, D., Yang, R., Booth, T.J., Geim, A.K., Making graphene visible, Appl. Phys. Lett. **2007,** 91, 063124-063126

13. Murbach, H. P., and Wilman, H., The origin of Stress in Metal Layers Condensed from the Vapour in High Vacuum, Proc. Phys. Soc. B **1953**, 66, 905-910

14. Wilman, H., The Temperatures attained at the Surfaces of Growing Deposits, and the Origin of Stress in Deposits, Proc. Phys. Soc. **1955**, 68 B, 474-476

15. Story, H.S., and Hoffman, R.W., Stress Annealing in Vacuum Deposited Copper Films, Proc. Phys. Soc. **1957**, 70 B, 950

16. Ferrari, A.C., Meyer, J.C., Scardaci, V., Casiragi, C., Lazzeri, M., Mauri, F., Piscanec, S., Jiang, D., Novoselov, K.S., Roth, S., Geim, A.K., Raman Spectrum of Graphene and Graphene Layers, Phys. Rev. Lett. 2006, 97, 187401-187404

17. Mohiuddin, T.M.G., Lombardo, A., Nair, R.R., Bonetti, A., Savini, G., Jalil, R., Bonini, N., Basko, D.M., Galiotis, C., Marzari, N., Novoselov, K.S., Geim, A.K., Ferrari, A.C., Uniaxial strain in graphene by Raman spectroscopy: G peak splitting, Grüneisen parameters, and sample orientation, Phys. Rev. B **2009**, 79, 205433-205440

18. Liu, F., Ming, P., Li, J., *Ab initio* calculation of ideal strength and phonon instability of graphene under tension, Phys. Rev. B **2007**, 76, 064120-064126

19. Bao, W., Miao, F., Chen, Z., Zhang, H., Jang, W., Dames, C., Lau, C.N., Controlled ripple texturing of suspended graphene and ultrathin graphite membranes, Nat Nanotechnol. **2009**, 4, 562-566

20. Cerda, E., Mahadevan, L., Geometry and Physics of Wrinkling, Phys. Rev. Lett. **2003**, 90, 074302

21. Peres, N.M.R., The transport properties of graphene: An introduction, Rev. Mod. Phys. **2010**, 82, 2673-2700

22. Das Sarma, S., Adam, S., Hwang, E.H., and Rossi, E., Electronic transport in two-dimensional graphene, Rev. Mod. Phys. **2011**, 83, 407-470

23. Zhou, Y.-B., Han, B.-H., Liao, Z.-M., Wu, H.-C., and Yu, D.-P., From positive to negative magnetoresistance in graphene with increasing disorder, Appl. Phys. Lett. **2011**, 98, 222502-222504

24. Kvashnin, A. G., Sorokin, P. B., and Yakobson, B. I., Flexoelectricity in carbon nanostructures: Nanotubes, Fullerenes, and Nanocones, J. Phys. Chem. Lett. **2015**, 6, 2740-2744

25. Suzuura, H., and Ando, T., Phonons and electron-phonon scattering in carbon nanotubes, Phys. Rev. B **2002**, 65, 235412-235426

26. Manes, J. L., Symmetry-based approach to electron-phonon interactions in graphene, Phys. Rev. B **2007**, 76, 045430-045439

27. Tombros, N., Jozsa, C., Popinciuc, M., Jonkman, H. T., and van Wees, B. J., Electronic spin transport and spin precession in single graphene layers at room temperature, Nature **2007**, 448, 571-574

28. Huertas-Herbando, D., Guinea, F., and Brataas, Spin-Orbit-Mediated Spin Relaxation in Graphene, Phys. Rev. Lett. **2009**, 103, 146801-146804

Table of Contents Graphic.

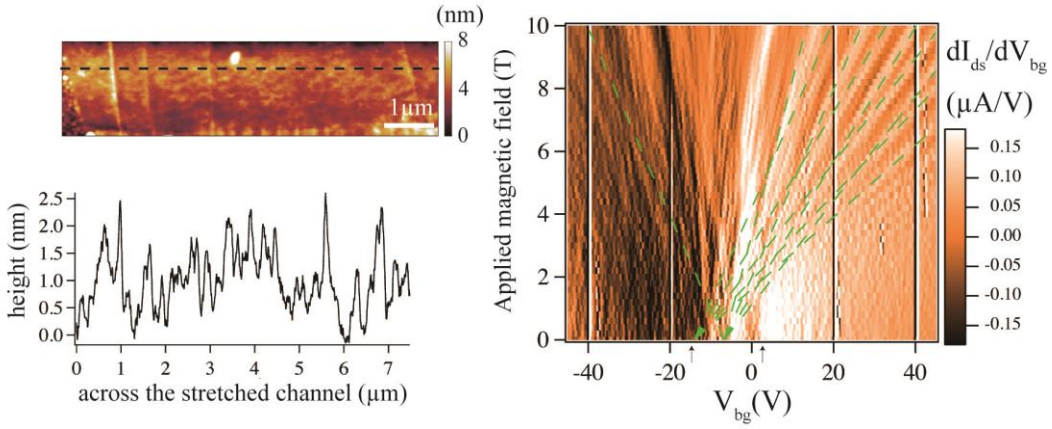
(nm)
8
4
0
1 μm
height (nm)
2.5
2.0
1.5
1.0
0.5
0.0
0 1 2 3 4 5 6 7
across the stretched channel (μm)
Applied magnetic field (T)
10
8
6
4
2
0
-40 -20 0 20 40
V_bg(V)
dI_ds/dV_bg
(μA/V)
0.15
0.10
0.05
0.00
-0.05
-0.10
-0.15